36. S. Paine-Saunders, B. L. Viviano, S. Saunders, *Genomics* **57**, 455 (1999).
37. S. Brown, J. Russo, D. Chitayat, D. Warburton, *Am. J. Hum. Genet.* **57**, 859 (1995).
38. M. Ramalho-Santos, D. A. Melton, A. P. McMahon, *Development* **127**, 2763 (2000).
39. C. Chiang *et al.*, *Nature* **383**, 407 (1996).
40. S. A. Brown *et al.*, *Nature Genet.* **20**, 180 (1998).
41. F. Cole, R. S. Krauss, *Curr. Biol.* **13**, 411 (2003).
42. N. Denef, D. Neubuser, L. Perez, S. M. Cohen, *Cell* **102**, 521 (2000).

43. We thank A. Kaykas and R. Moon for providing the Super TopFlash reporter; F. Weiss-Garcia and the Sloan-Kettering Hybridoma Core Facility (NY) for development of monoclonal antibodies; R. Gong for technical assistance; S. Celniker for help with annotation of DGCr1; R. L. Johnson and S. M. Cohen for antibodies; S. Zusman at Genetic Services (MA) for help with *dally* dsRNA embryo injections; and J. Taipale for critical review of the manuscipt. Supported by grants and fellowships from NIH and a Life Sciences Research Foundation Fellowship (L.L.). P.A.B. is an investigator of the Howard Hughes Medical Institute.

Supporting Online Material
www.sciencemag.org/cgi/content/full/299/5615/2039/DC1
Materials and Methods
Fig. S1
Tables S1 and S2
References

11 December 2002; accepted 6 March 2003

REPORTS

Polymer Replicas of Photonic Porous Silicon for Sensing and Drug Delivery Applications

Yang Yang Li,[1] Frédérique Cunin,[1] Jamie R. Link,[1] Ting Gao,[1] Ronald E. Betts,[1] Sarah H. Reiver,[1] Vicki Chin,[2] Sangeeta N. Bhatia,[2] Michael J. Sailor[1]

Elaborate one-dimensional photonic crystals are constructed from a variety of organic and biopolymers, which can be dissolved or melted, by templating the solution-cast or injection-molded materials in porous silicon or porous silicon dioxide multilayer (rugate dielectric mirror) structures. After the removal of the template by chemical dissolution, the polymer castings replicate the photonic features and the nanostructure of the master. We demonstrate that these castings can be used as vapor sensors, as deformable and tunable optical filters, and as self-reporting, bioresorbable materials.

Synthesis of materials using nanostructured templates has emerged as a useful and versatile technique to generate ordered nanostructures (*1*). Templates consisting of microporous membranes (*2*, *3*), zeolites (*4*), and crystalline colloidal arrays (*5*–*7*) have been used to construct elaborate electronic, mechanical, or optical structures. Porous Si is an attractive candidate for use as a template (*8*) because the porosity and average pore size can be tuned by adjusting the electrochemical preparation conditions that allow the construction of photonic crystals, dielectric mirrors, microcavities, and other optical structures (*9*). For many applications, porous Si is limited by its chemical and mechanical stability. The use of porous Si as a template eliminates these issues while providing the means for construction of complex optical structures from flexible materials that are compatible with biological systems or harsh environments.

Multilayered porous Si templates containing nanometer-scale pores are prepared (*10*) by an anodic electrochemical etch of crystalline silicon wafers with the use of a pseudosinusoidal current-time waveform, according to published procedures (*9*, *11*–*16*). The thickness, pore size, and porosity of a given layer is controlled by the current density, duration of the etch cycle, and etchant solution composition (*17*). The multilayer templates possess a sinusoidally varying porosity gradient, providing sharp features in the optical reflectivity spectrum (Fig. 1) that approximate a rugate filter (*18*). The porous Si is converted to porous SiO_2 by thermal oxidation, and the oxidized nanostructure (fig. S1) (*10*) is used as a template for solution-cast or injection-molded thermoplastic polymers.

Removal of the porous SiO_2 template from the polymer or biopolymer imprint by chemical dissolution provides a freestanding porous polymer film with the optical characteristics of the photonic crystal master (figs. S2 to S4). Reflection spectroscopy (Fig. 1) and scanning electron microscopy (SEM) (Fig. 2) confirm that the photonic structure of the porous Si master is retained in the polymer casting. The sharp optical reflectivity feature expected of a rugate filter is observed in both the template and the polymer casting (Fig. 1), confirming that the process replicates the microstructure. Cross-sectional SEM measurements (Fig. 2 and fig. S5) corroborate the optical data.

Vapor dosing experiments confirm that the microporous nanostructure is retained in the castings. The position of the spectral feature for a rugate filter depends on the periodicity and refractive index gradient of the structure. When porous Si multilayers are exposed to condensable vapors such as ethanol or hexane, microcapillary condensation in the nanometer-scale pores produces an increase in the average refractive index of the matrix and a spectral red shift of the photonic feature (*11*, *19*, *20*). The shift of the spectral peak correlates with partial pressure of the analyte in the gas stream, following the Kelvin equation for condensible vapors (*15*, *19*–*21*). Dose-response curves for ethanol vapor for the porous Si template and for the polystyrene

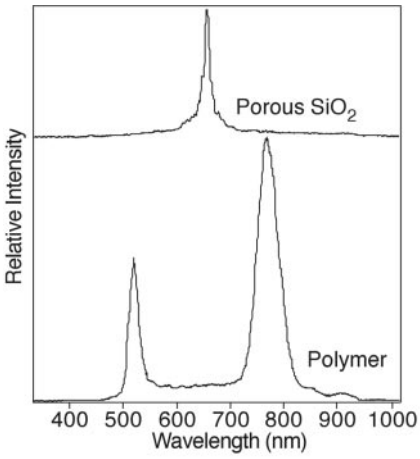

Fig. 1. Reflectivity spectra of an oxidized porous Si rugate film (top) and a polystyrene film cast from the porous Si template (bottom). The spectral peaks correspond to the second-order diffraction peak of the template and the second- and third-order diffraction peaks of the imprint. The porous Si template was etched using a sinusoidal current varying between 38.5 and 192.3 mA/cm^2, with 70 repeats and a periodicity of 8 s. The total thickness of the porous Si film is 40 μm. The reflected light spectra were obtained using an Ocean Optics SD2000 charge-coupled device spectrometer using tungsten light illumination. Spectra are offset along the *y* axis for clarity.

[1]Department of Chemistry and Biochemistry, University of California, San Diego, 9500 Gilman Drive, Department 0358, La Jolla, CA 92093–0358, USA. [2]Department of Bioengineering, University of California, San Diego, 9500 Gilman Drive, Department 0412, La Jolla, CA 92093–0412, USA.

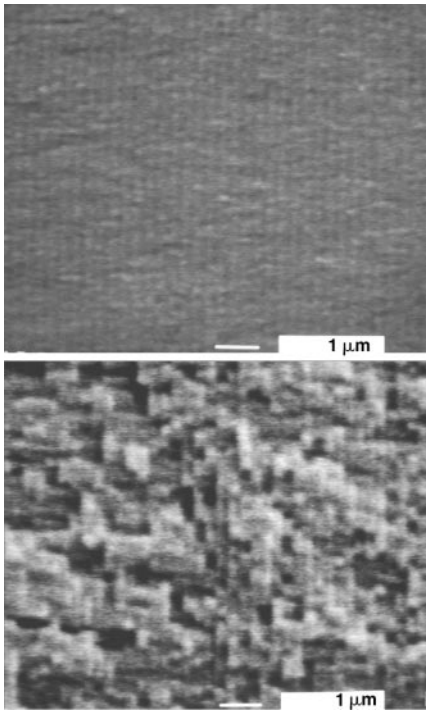

Fig. 2. Cross-sectional scanning electron micrograph (secondary electron image) of the porous silicon template (**top**) and a polystyrene film cast from a similar template (**bottom**). Samples were prepared using identical procedures as those used for the samples represented in Fig. 1, except that the porous silicon film was etched using a sinusoidal current varying between 11.5 and 192.3 mA/cm^2, with 70 repeats and a periodicity of 5 s. Scale bar, 1 μm.

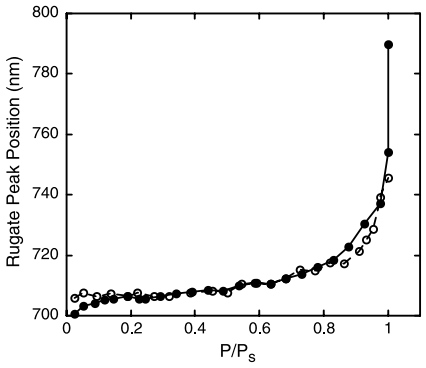

Fig. 3. Dose-response curves for a porous Si rugate film template (solid circles, solid line) and its replicate polystyrene film (open circles, dashed line) upon exposure to ethanol vapor. The data are presented as the wavelength of the second-order peak maximum from the rugate structure as a function of P/P$_s$, where P is the partial pressure of ethanol and P$_s$ is the saturation vapor pressure of ethanol (44 torr). The samples were prepared in a similar way to those whose spectra are presented in Fig. 1.

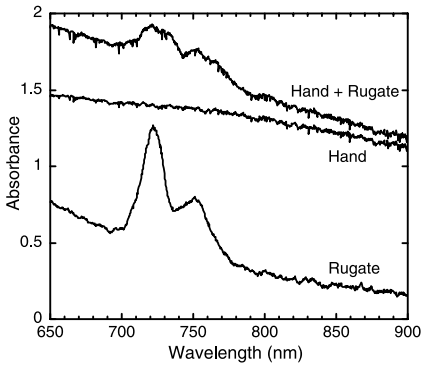

Fig. 4. Absorption spectrum (transmission mode) of a porous Si rugate filter (bottom, rugate), 1 mm of human hand tissue (hand), and the porous Si rugate filter measured through 1 mm of human hand tissue (rugate + hand). The figure demonstrates the ability to monitor the spectral signature of the nanostructured materials in vivo. The spectra hand and rugate + hand are offset along the *y* axis by +0.8 absorbance units for clarity.

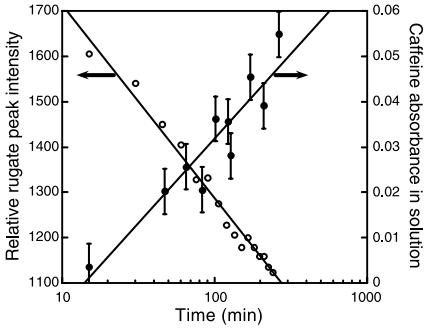

Fig. 5. Intensity of reflected light from the polymer rugate structure [measured at 533 nm (open circles)] and UV absorbance of free caffeine in the solution [measured at 274 nm (solid circles)] as a function of time for a caffeine-impregnated PL casting immersed in aqueous solution (pH = 10).

casting both display a large relative response at partial pressures within a few percent of the saturation vapor pressure (Fig. 3), characteristic of capillary condensation in nanometer-scale pores (*19*, *20*). Imprints prepared from melt-cast polyethylene display the optical spectrum characteristic of the rugate structure, but they show no spectral shift upon exposure to ethanol vapor. Presumably, the more viscous molten polyethylene does not impregnate the porous SiO_2 sufficiently enough to replicate the nanometer-scale features that are required to generate microcapillary condensation effects, as occurs with the solution-cast material.

Biocompatible and bioresorbable polymers are of great interest for their use in prosthesis, medical suture, tissue engineering, and drug delivery systems. Biodegradable polyesters are the most widely studied and used polymers for application in the controlled release of drugs (*22*). In some cases, there is a desire to monitor the status of the biomaterial in vivo. Because the spectral reflectance peaks of the porous Si filters and their polymer castings can be tuned over a wide range (from at least 400 to 10,000 nm), the peaks can be placed at wavelengths corresponding to a region of relatively low absorption in human tissue. The spectrum of a porous Si photonic structure that exhibits two resonances, obtained through 1 mm of soft tissue of a human hand (Fig. 4), demonstrates that such measurements could be obtained in vivo. The measurement of the decay in intensity of the rugate peak could thus be used to monitor, for example, the release of drug from an implanted biocompatible polymer.

To test the above hypothesis, we prepared a caffeine-impregnated poly(L-lactide) (PL) film, cast from a thermally oxidized porous silicon rugate template. Replication of the optical spectrum was observed in the biocompatible polymer upon removal of the porous silicon template. The photonic structure in the film degraded completely in about 5 days in a pH 10 aqueous buffer solution. The intensity of the rugate peak displays an approximately exponential decay over the first 3 days, reflecting the progressive hydrolysis of the biopolymer in the aqueous environment (fig. S6). Simultaneous measurement of the decay of the rugate peak and the appearance of caffeine in the solution (caffeine absorption occurs at 274 nm) confirms that the drug is released on a time scale comparable to polymer degradation (Fig. 5).

Castings made from flexible polymers such as polydimethylsiloxane (solution cast) or polyethylene (melt cast) provide mechanically deformable filters (fig. S7). Deformation of the material by application of a moderate compressive stress produces a spectral blue shift (by a few nanometers) in the photonic feature, consistent with a decrease in the layer spacing of the rugate filter. The chemical and mechanical instability of porous Si has been identified as a considerable limitation for biological and environmental sensor applications. Because the castings possess the chemical and mechanical properties of the polymers used, the approach presented here provides a substantial improvement in the design of experiments and devices using nanostructured photonic materials but retains the simplicity of fabrication inherent in the electrochemical synthesis of porous Si.

References and Notes

1. S. Polarz, M. Antonietti, *J. Chem. Soc. Chem. Commun.* **2002**, 2593 (2002).
2. M. Wirtz, M. Parker, Y. Kobayashi, C. R. Martin, *Chem. Eur. J.* **16**, 3572 (2002).
3. J. C. Hulteen, C. R. Martin, *J. Mater. Chem.* **7**, 1075 (1997).
4. K. Moller, T. Bein, *Chem. Mater.* **10**, 2950 (1998).
5. C. E. Reese, M. E. Baltusavich, J. P. Keim, S. A. Asher, *Anal. Chem.* **73**, 5038 (2001).
6. X. Xu, S. A. Majetich, S. A. Asher, *J. Am. Chem. Soc.* **124**, 13864 (2002).
7. C. L. Haynes, R. P. Van Duyne, *J. Phys. Chem. B* **105**, 5599 (2001).
8. S. Matthias *et al.*, *Adv. Mater.* **14**, 1618 (2002).
9. M. Thonissen, M. G. Berger, in *Properties of Porous Silicon*, L. Canham, Ed. (Short Run Press, London, 1997), vol. 18, pp. 30–37.
10. Materials and methods are available as supporting material on *Science* Online.
11. T. A. Schmedake, F. Cunin, J. R. Link, M. J. Sailor, *Adv. Mater.* **14**, 1270 (2002).
12. F. Cunin *et al.*, *Nature Mater.* **1**, 39 (2002).
13. V. Lehmann, R. Stengl, H. Reisinger, R. Detemple, W. Theiss, *Appl. Phys. Lett.* **78**, 589 (2001).

14. L. Pavesi, P. Dubos, *Semicond. Sci. Tech.* **12**, 570 (1997).
15. P. A. Snow, E. K. Squire, P. S. J. Russell, L. T. Canham, *J. Appl. Phys.* **86**, 1781 (1999).
16. G. Vincent, *Appl. Phys. Lett.* **64**, 2367 (1994).
17. A. Halimaoui, in *Properties of Porous Silicon*, L. Canham, Ed. (Short Run Press, London, 1997), vol. 18, pp. 12–22.
18. M. G. Berger *et al.*, *Thin Solid Films* **297**, 237 (1997).
19. S. Zangooie, R. Bjorklund, H. Arwin, *Sens. Actuators B* **43**, 168 (1997).
20. J. Gao, T. Gao, Y. Li, M. J. Sailor, *Langmuir* **18**, 2229 (2002).
21. P. Allcock, P. A. Snow, *J. Appl. Phys.* **90**, 5052 (2001).
22. K. E. Uhrich, S. M. Cannizzaro, R. S. Langer, K. M. Shakesheff, *Chem. Rev.* **11**, 3181 (1999).
23. The authors thank J. Dorvee for helpful discussions and S. A. Cybart, K. Chen, and R. C. Dynes for assistance with the electron microscope measurements. Supported by the David and Lucile Packard Foundation, the NSF, and the Air Force Office of Scientific Research (grant F49620-02-1-0288).

Supporting Online Material
www.sciencemag.org/cgi/content/full/299/5615/2045/DC1
Materials and Methods
Figs. S1 to S7

9 December 2002; accepted 20 February 2003

Microscopic Dynamics of Liquid Aluminum Oxide

H. Sinn,[1] B. Glorieux,[2] L. Hennet,[3] A. Alatas,[1] M. Hu,[1] E. E. Alp,[1] F. J. Bermejo,[4] D. L. Price,[3] M.-L. Saboungi[5]*

Collective excitations have been observed in liquid aluminum oxide at high temperatures by combining a containerless sample environment with inelastic x-ray scattering. The excitation spectra show a well-defined triplet peak structure at lower wave vectors *Q* (1 to 6 nanometers^{-1}) and a single quasi-elastic peak at higher *Q*. The high-*Q* spectra are well described by kinetic theory. The low-*Q* spectra require a frequency-dependent viscosity and provide previously unknown experimental constraints on the behavior of liquids at the interface between atomistic and continuum theory.

The dynamics of liquids are reasonably well understood in two regimes of length scale: in the continuum limit (length scale $\gg$ interparticle distance), where hydrodynamic theory can be applied, and in the short-wavelength regime (length scale $\sim$ interparticle distance), where kinetic theory can be extended to liquid densities. The intermediate region, corresponding to a small but finite number of interparticle distances, remains a challenge for modern statistical physics (*1*–*3*). The dynamics of ionic liquids such as molten salts provide a potentially rich field for coupling experiments and theory because two classes of fluctuations, density and charge, can be observed by inelastic neutron scattering and light scattering measurements. However, the kinematic restrictions of neutron scattering make it impossible to reach acoustic modes over a certain range of wave vector Q, and the high-temperature regime is inaccessible by light scattering because the inelastic signal is obscured by the black-body radiation. The recently developed high-resolution inelastic x-ray scattering (IXS) technique goes beyond these limitations as evidenced by results obtained on liquid metals, water, and organic liquids (*4*).

Here, we apply IXS to an oxide melt whose electrical transport properties classify it as a molten salt (*5*, *6*). Aluminum oxide was chosen because many of its physical properties and structure have been determined in the molten and supercooled states (*7*–*9*). The measurements were performed in a containerless environment. Alumina spheres 3 to 4 mm in diameter were suspended in an oxygen gas jet and heated with a 270-W CO_2 laser beam to temperatures between 2300 and 3100 K. Carefully adjusted gas flow through a conical nozzle maintained the levitated sample at a position stable within ± 20 μm above the plane of the top edge of the nozzle, allowing a clear path for the incident and diffracted x-ray beams. The temperature was measured by a pyrometer directed at the point illuminated by the x-ray beam (*10*). The IXS measurements were carried out at the 3ID-C beamline at the Advanced Photon Source, with an inline monochromator consisting of two nested channel-cut crystals and a back scattering analyzer setup in the horizontal scattering plane 6 m from the

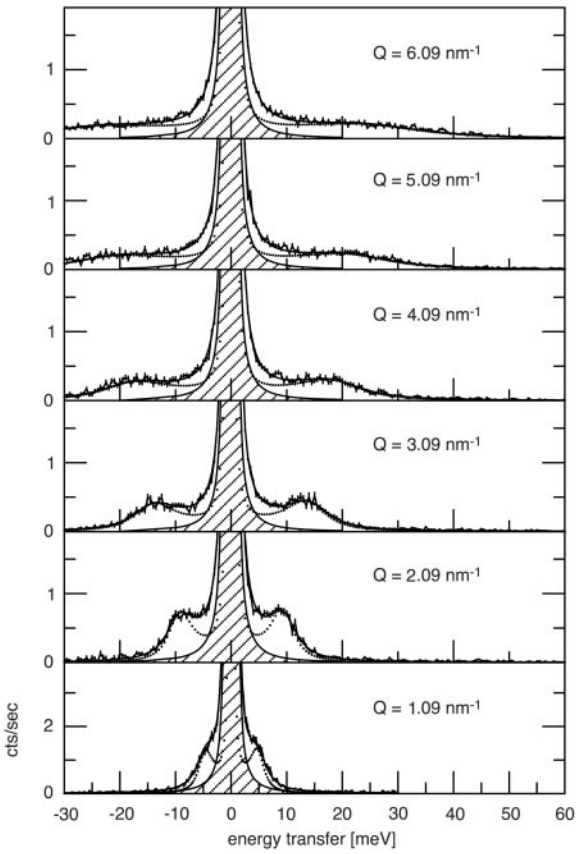

Fig. 1. Inelastic x-ray scattering spectra, $I(Q, \omega)$, for liquid Al_2O_3 at the six lowest wave vectors measured and a temperature of 2323 K. The fits of Eq. 3 are shown as solid lines, and the equivalent functions with the resolution function deconvoluted are shown as dotted lines. The resolution function is shown hatched. cts, counts.

[1]Advanced Photon Source, Argonne National Laboratory, Argonne, IL 60439, USA. [2]Institut de Science et de Génie des Materiaux et Procédés, 66100 Perpignan Cedex, France. [3]Centre de Recherche sur les Matériaux à Hauts Températures, Centre National de la Recherche Scientifique (CNRS), 45071 Orleans Cedex 2, France. [4]Consejo Superior de Investigaciones Científicas, Department of Electricity and Electronics, University of the Basque Country, 48080 Bilbao, Spain. [5]Centre de Recherche sur la Matière Divisée, CNRS, University of Orleans, 45071 Orleans Cedex 2, France.

*To whom correspondence should be addressed. E-mail: mls@cnrs-orleans.fr